Volume 1 | Number 1 | Jan 2013 | Pages 1–100

Soft Matter

www.rsc.org/softmatter

ROYAL SOCIETY OF CHEMISTRY

ROYAL SOCIETY OF CHEMISTRY

www.rsc.org/softmatter

A microgel artificial glutathione peroxidase with high catalytic activity and efficient preparing process was prepared based on supramolecular host-guest self-assembly. It was proved that both the hydrophobic microenvironment and the crosslinker in supramolecular microgel network played significant roles in enhancing and altering the temperature responsive catalytic behavior.
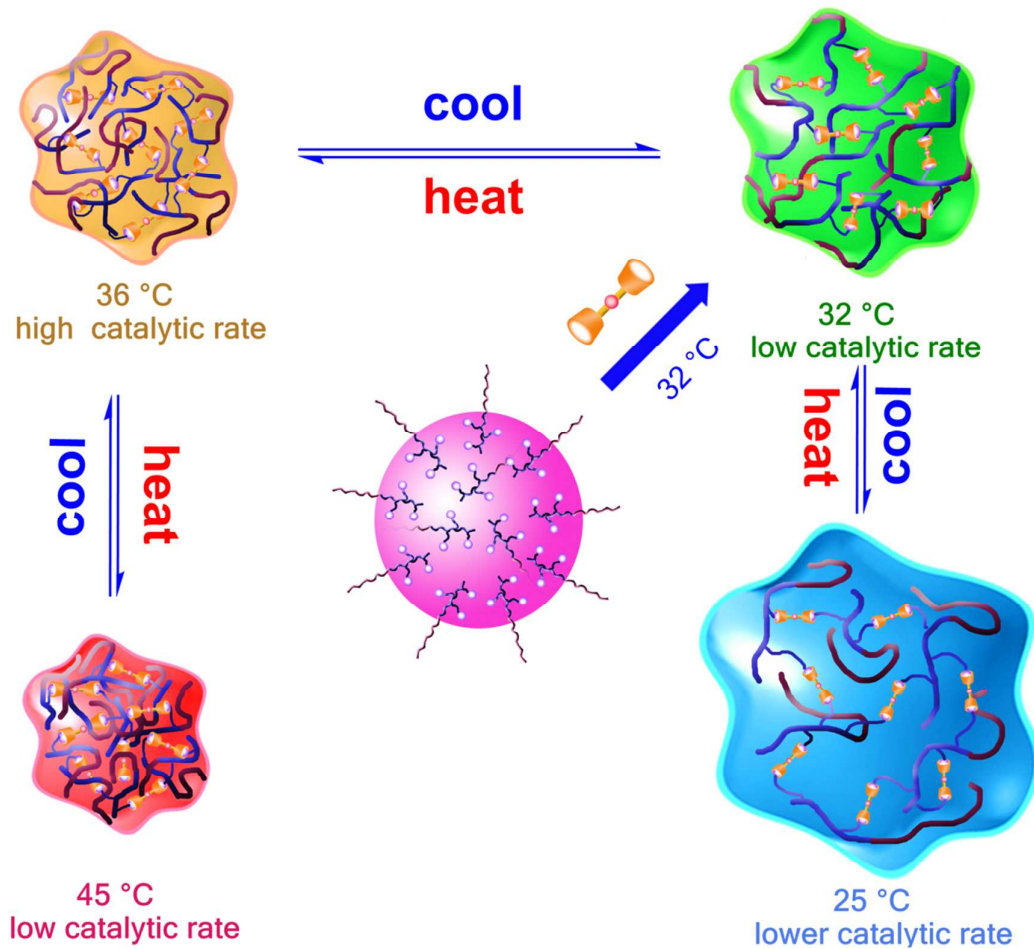
ARTICLE TYPE

Construction of a smart microgel glutathione peroxidase mimic based on supramolecular self-assembly

Yanzhen Yin,[a,b] Shufei Jiao,[b*] Ruirui Zhang,[b] Xiaoxi Hu,[b] Zhongfeng Shi,[b] Zuqiang Huang,[a] *

In an effort to construct smart artificial glutathione peroxidase (GPx)featuring high catalytic activity in an efficient preparing process, an artificial microgel GPx (**PPAM-ADA-Te**) has been prepared using a supramolecular host-guest self-assembly technique. Herein, 6,6'-Telluro-bis(6-deoxy-β-cyclodextrin) (**CD-Te-CD**) was selected as a tellurium-containing host molecule, which also served as the crosslinker
10 for the scaffold of the supramolecular microgel. And adamantane-containing block copolymer (**PPAM-ADA**) was designed and synthesized as guest building block copolymer. Subsequently, **PPAM-ADA-Te** was constructed through self-assembly of **CD-Te-CD** and **PPAM-ADA**. The formation of this self-assembled construct was confirmed by Dynamic Light Scattering, NMR, SEM and TEM. Notably, **PPAM-ADA-Te** not only exhibits a significant temperature responsive catalytic activity, but also
15 features the characteristic saturation kinetics behaviour, similar to that of a natural enzyme catalyst. We demonstrate in this paper that both the hydrophobic microenvironment and the crosslinker in this supramolecular microgel network played significant roles in enhancing and altering the temperature responsive catalytic behaviour. The successful construction of **PPAM-ADA-Te** not only provides a novel method for the preparation of microgel artificial GPx with high catalytic activity but also provides
20 properties suitable for the future development of intelligent antioxidant drugs.

Introduction

As one of the by-products in the metabolism cells, reactive oxygen species (ROS) have two different effects on human organisms. An excess of ROS may lead to a variety of oxidative
25 stress-related diseases such as reperfusion injury, inflammation, neuronal apoptosis, and cancer[1, 2]. However, ROS in a physiologically appropriate amount has been found to play a critical role in cell signalling and homeostasis[3]. The antioxidative defense system, particularly the antioxidative enzyme system,
30 plays a vital role in the control of the correct amount of ROS. Typically, (GPx, Ec.1.11.1.9) proves to be an important selenium-containing enzyme catalyzing the reduction of a hydroperoxide species (e.g. ROOHs) using glutathione (GSH) as a substrate[4, 5]. Due to its biologically significant role, recent
35 efforts have been focussed on the production of organoselenium/tellurium compounds that could mimic the property of GPx in recent years. Typically, proteins[16, 20, 23, 31, 33], hyperbranched polymers[22, 32, 34, 35], dendrimers[19, 36], ebselen-like selenoxides[21, 24, 26], switchable supramolecular architectures[25, 29,
40 37-40], selenopeptides[28, 41], cyclodextrin derivatives[12, 42-44], micelles or vesicles[45-48] are being as functional scaffold to construct various organoselenium/tellurium compounds. In the light of the structural parameters of GPx, a variety of artificial GPxs have already been prepared in our group, employing imprinting
45 methods[13], self-assembly method[17, 40], ATRP techniques[49, 50], and

blending processes[18,51].

The first example of a microgel, cross-linked polymer particle, has been described by Staudinger[52]. By combining the unique property of the characteristics of linear macromolecules with a
50 three-dimensional network, microgels have been used for the development of these novel biomaterials[53, 54]. For example, such polymer microgels have already been widely employed in the field of artificial enzymes[49, 53], in regenerative medicine[55], as sensor[56], drug delivery system[57], etc. Furthermore, microgels
55 feature key requirement for the design of artificial enzymes. The three-dimensional space network of microgels proves to be similar to the folding secondary structure of native enzyme. Therefore, a variety of artificial enzymes have been constructed employing microgel motif[49, 53, 58, 59]. We previously reported the
60 production of an artificial GPx based on a temperature-responsive microgel using poly(*N*-isopropylacrylamide) (PNIPAM) as framework (here, designated **Microgel GPx**)[49]. **Microgel GPx** exhibited catalytic ability that proved to be controllable and could be potentially applied in the exploration of intelligent antioxidant
65 drug responsible for the adjustment of ROS *in vivo*. However, in this work the efficient separation of cetyltrimethyl ammonium bromide (CTAB) from **Microgel GPx** solution could not be achieved. Furthermore, the high molecular weight of **Microgel GPx** may lead to difficultly degradation or metabolic
70 elimination[60-62]. Therefore, in an effort to overcome these two obstacles, we designed a modified microgel and changed the covalently crosslinked motif to form a non-covalently crosslinked

supramolecular microgel. Here, renamed this new microgel as **SM-Te**[17]. Unfortunately, even though **SM-Te** features a superior supramolecular microgel scaffold compared to **Microgel GPx**, the maximum catalytic rate of **SM-Te** regrettably decreased by 30.5%(5.60 μM·min^{-1} at 38°C[17]). The maximum catalytic rate of **Microgel GPx $_{max}$** was shown to be 8.09 μM·min^{-1} at 32°C[49]. Therefore, we devote efforts to the exploration of novel smart artificial GPx, featuring both an excellent supramolecular microgel scaffold as well as an improved catalytic rate. Noticeably, in our previous research, the length of the hydrocarbon chain in the micelle artificial GPx displayed a key parameter in altering the exact match of elements and further enhancing the catalytic activity[46]. Continuing this work, we envisioned further designs for microgel GPx with an optimum crosslinker. Investigating the influence mechanisms of the crosslinker together with the catalytic activity are crucial studies need to design artificial GPx.

Here, a novel supramolecular microgel artificial GPx, **PPAM-ADA-Te**, has been designed and synthesized based on the self-assembly behaviour of **CD-Te-CD** and **PPAM-ADA**. Notably, although the self-assembled behaviour of **PPAM-ADA-Te** was similar to that of **SM-Te** and **Microgel GPx**, the catalytic activity of **PPAM-ADA-Te** were significantly increased by 222.5%(compared to **SM-Te**) and 123.2% (compared to **Microgel GPx**), respectively. As highlighted in subsequent sections, both the hydrophobic microenvironment as well as the crosslinker in the supramolecular microgel network played crucial roles in enhancing and altering the temperature responsive catalytic behaviour. The successful preparation of **PPAM-ADA-Te** not only provides a novel method for the preparation of microgel artificial GPx with high catalytic activity but also offers a material with fascinating properties for the design of novel intelligent antioxidant drugs.

Experimental Section

Materials.

Tris(2-dimethylaminoethyl)amine (Me$_6$TREN) was synthesized as described previously[63]. *N*-isopropylacrylamide(NIPAM, Aldrich) was recrystallized from hexane and toluene, and dried under vacuum prior to use. Sodium borohydride and 3-bromo-1-propanol were purchased from Fluka and were used without further purification. Acrylamide, *β*-cyclodextrin, tellurium powder, adamantane-1-carboxylic acid, phenyl methanol and 4-toluene sulfonyl chloride were purchased from Nanning Lantian Reagent Co. Triethylamine and tetrahydrofuran were purchased from Nanning Lantian Reagent Co. and rigorously dried with sodium. Acryloyl chloride, thionyl chloride and 2-bromopropanoly bromide were purchased from Anhui Wotu Reagent co. 3-carboxyl-4-nitrobenzenethiol (TNB) was synthesized from 5,5'-dithiobis(2-nitrobenzoic acid) as described previously[12]. 1-[p-(phenyl-azo) phenoxyethyl]pyridinium bromide (AZO) was synthesized according to the previous report[64]. Benzyl 2-bromopropanoate was synthesized according to the previous report[51]. 6,6'-Telluro-bis(6-deoxy-β-cyclodextrin) (**CD-Te-CD**) was synthesized according to the previous report[65].

Instrumentations.

The NMR characterization was performed with Bruker 300 MHz spectrometer using a TMS proton signal as the internal standard. UV-vis spectra were obtained using a Shimadzu 2600 UV-vis spectrophotometer. Scanning electron microscopy (SEM) observations were carried out on a JEOL JSM-6700F scanning electron microscope with primary electron energy of 3 kV. Transmission electron microscopy (TEM) observations were carried out on a JEOL JEM 3010 transmission electron microscope. The buffer pH values were determined with a METTLER TOLEDO 320 pH meter. Dynamic Light Scattering (DLS) experiments were performed at Malven ZETAS12-ERNANOSERIES instrument. Molecular weights and molecular weight distributions were determined by Waters 515 Gel Permeation Chromatography using THF as eluent at a flow rate of 1.0 mL/min.

Synthesis of ADA-monomer

Adamantane-1-carboxylic acid (1.803 g, 0.010 mol) was dissolved in 4 mL of thionyl chloride. After the mixture was stirred for 4 h at 60°C, thionyl chloride was removed by distillation and 1-adamantanecarbonyl chloride (1.98 g, 0.010 mol) was obtained. Then, 1-adamantanecarbonyl chloride was dissolved in 40 mL of anhydrous tetrahydrofuran and added dropwise to a stirred solution of tetraethylene glycol (1.94 g, 0.010 mol) and triethylemine (1.52 mL, 0.011 mol) in 120 mL anhydrous tetrahydrofuran at 0°C. The mixture was stirred for 20 h at room temperature. The precipitate was filtered and the filtrate was concentrated under vacuum. The product (tetraethylene glycol monoadamantane-1-carboxylate) was purified by silica gel flash chromatography (elution with ethyl acetate) to give 3.21 g (yield of 90%) as a viscous colorless oil.

Then, acryloyl chloride (0.65 mL, 0.008 mol) was dissolved in 20 mL of anhydrous tetrahydrofuran and added dropwise to a stirred solution of tetraethylene glycol monoadamantane-1-carboxylate (2.85g, 0.008 mol) and triethylmine (1.24 6 mL, 0.009 mol) in anhydrous tetrahydrofuran (60 mL) at 0°C. After completing addition, the mixture was stirred for 3 h at room temperature and the precipitated was filtered. The filtrate was concentrated under vacuum, the product was chromatographed (petroleum ether/ethyl acetate, 1:3) to give 2.90 g (yield of 88%) of **ADA-monomer** as a buff oil.

ADA-monomer: ^{1}H NMR (300 MHz, CDCl$_3$) δ (ppm)5.82-6.46(3 H, CH$_2$═CH─), 4.33-4.30(t, 2 H, (acrylate) COOCH$_2$─), 4.22-4.19(t, 2 H, (adamantane-1-carboxylate) COOCH$_2$─), 3.76-3.65(m, 12 H, glycol), 2.01 (s, 3 H, adamantane), 1.89 (s, 6 H, adamantane),1.71 (s, 6 H, adamantane)

Synthesis of PPAM-ADA

The synthesis of **PPAM-ADA** was similar to the synthesis of **PPAM-CD** in our previous report[17], except the **CD-monomer** was replaced by **ADA-monomer**. GPC analysis of **PPAM-ADA** revealed a M$_n$ of 13070, M$_w$ of 16290 and a polydispersity, Mw/Mn, of 1.25. The concentration of adamantane in the **PPAM-ADA** was estimated to be $3.3×10^{-4}$ mmol/mg according to NMR analysis.

LCST Determination of PPAM-ADA

The optical transmissions of **PPAM-ADA** solution (1 mg·mL^{-1}) at different temperatures were measured at 600 nm using a Shimadzu 2600 UV-vis spectrophotometer. Sample cells were

thermostated in a circulator bath at different temperatures from 25 to 45°C prior to the measurements. The LCST was defined as the temperature at the inflection point in the plot of light transmission as a function of temperature. The LCST of **PPAM-**
5 **ADA** was 32.2°C.

Preparation of supramolecular microgel PPAM-ADA-Te

Deionized water (9.0 mL) was introduced into a 25 mL flask, **CD-Te-CD** (2.85 mg, 0.005 mmol) was added and solved in it. **PPAM-ADA (**33 mg, 0.01 mmol**)** was solved in DMF (1.0 mL).
10 The solution of **PPAM-ADA** was thermostated in a circulator bath at 32°C for 20 min. Then, the DMF solution of **PPAM-ADA** was slowly added into the solution of **CD-Te-CD** under sonication at 32°C. After the dropwise process was finished, the mixture solution was treated under continual sonication at 32°C
15 for 1 h. Then, the supramolecular microgel **PPAM-ADA-Te** was obtained with the concentration of 3.58 mg·mL^{-1}. And the concentration of tellurium (catalytic center of artificial GPx) was 0.5 mM.

LCST Determination of PPAM-ADA-Te

20 The determination of optical transmissions of **PPAM-ADA-Te (**1 mg·mL^{-1}**)** solution at different temperatures was measured using the similar method to that of **PPAM-ADA**. The LCST of **PPAM-ADA-Te** was 33.6°C.

Determination of GPx activity.

25 The catalytic activity was assayed according to a modified method reported by Hilvert et al[6]. Typically, the reaction was carried out at 25°C in a 1 mL quartz cuvette, 700 μL of phosphate buffer (pH=7.0. 50 mM) and 100 μL of the **PPAM-ADA-Te** (10 μM) were added, and then 100 μL of the TNB solution (1.5 mM)
30 was added. The mixture in the quartz cuvette was pre-incubated at appropriate temperature for 3 min. Finally, the reaction was initiated by the addition of 100 μL of cumene hydroperoxide (CUOOH) (2.5 mM), and the absorption decrease of TNB at 410 nm (ε_{410}=13600 M^{-1}·cm^{-1}. pH=7.0) was monitored using a
35 Shimadzu 2600 UV-vis spectrophotometer. Appropriate control of the non-enzymatic reaction was performed and was subtracted

from the catalyzed reaction.

Results and Discussion

Design of PPAM-ADA-Te

40 A proper physiological concentration of ROS is not harmful to the human organism and ROS play an important role in the metabolic cell signalling and homeostasis. However, an overproduction of ROS is associated with a variety of oxidative stress-related diseases. Smart artificial GPxs with controllable
45 catalytic abilities based on a block copolymer scaffold[18,49-51]and microgel scaffold (e.g. **SM-Te**[17] and **Microgel GPx**[49]) show promising properties that could be useful in development of intelligent antioxidant drug. As mentioned before, compared to covalently crosslinked artificial enzymes (e.g. **MicrogelGPx**),
50 **SM-Te** bearing a supramolecular microgel scaffold proved to be advantageous, however, the maximum catalytic rate significantly decreased. Therefore, we envisioned a structural design to achieve higher catalytic activity through modification of the crosslinker spacer. Ritter *et al.* already showed that the length of
55 the spacer is crucial for the water solubility of temperature responsive materials based on cyclodextrin complexes[66]. Furthermore, we believe that the maximum catalytic rate will be influenced in a similar way as the water solubility. This is why we focussed our efforts on modifying the length of the
60 corresponding crosslinker used.

As shown in Fig. 1, three types of crosslinker were used in this study. **Corsslinker 1** in **Microgel GPx** proves to be shorter and **Corsslinker 2** in **SM-Te** proves to be longer. **Corsslinker 3** in **PPAM-ADA-Te** proves to be of intermediate length, between
65 **Corsslinker 1** and **Corsslinker 2**. Remarkably, the catalytic activity of **PPAM-ADA-Te** were significantly increased by 222.5% and 124.1%, respectively. The investigation of the influence of the crosslinker on the catalytic activity in described in the subsection entitled *Catalytic mechanism of **PPAM-ADA-Te***. In
70 an effort to construct the scaffold of **PPAM-ADA-Te**, a series of functional molecules and polymers were used (cf. Fig. 2).
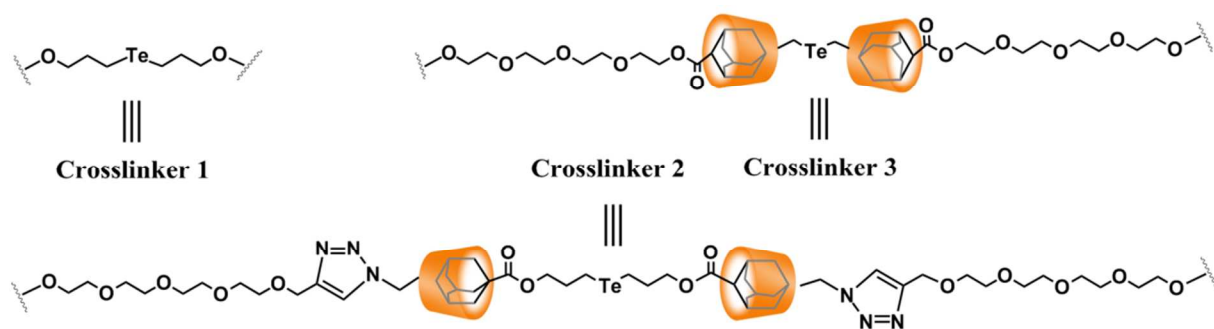

Fig. 1 The crosslinkers of smart artificial GPxs. **Corsslinker 1** was crosslinker of **Microgel GPx**[49]; **Corsslinker 2** was crosslinker of **SM-Te**[17]; **Corsslinker 3** was crosslinker of **PPAM-ADA-Te** in this work.

75 **NIPAM**, **AM** and an **ADA-monomer** were used as functional monomers. **PPAM-ADA** was prepared via Atom Transfer Radical Polymerization (ATRP), which generally proves to be an efficient medhod for the synthesis of block copolymers with a controlled structure[67, 68]. **NIPAM** in the scaffold of **PPAM-ADA**
80 results in a temperature responsive behaviour, whereas **AM**

functions as the hydrophilic block in the scaffold of **PPAM-ADA**. The **ADA-monomer** was used as the guest molecule moiety in **PPAM-ADA**, and was further employed to complex the host molecule (**CD-Te-CD**) via a self-assembly process.

85 The crystal structure of bovine erythrocyte GPx has been reported by Epp et al. in 1983[5]. The catalytic active site of GPx

has been well studied by mimicking the catalytic center of selenocysteine in GPx using various tellurium-containing complexes[7, 12, 46, 50, 51]. It turned out that tellurium-containing complexes was more efficient in artificial GPx as their selenium-containing analogues. Therefore, **CD-Te-CD**, a well-studied host artificial GPx[12, 65], was used to serve two purposes: (1) as an excellent alternative for selenocysteine in native GPx, (2) as intimate part of the crosslinker unit for the preparation of **PPAM-ADA-Te**. Additionally, **AZO** was useed as a competitive guest in order to confirm the successful formation of a supramolecular microgel via NMR assay.
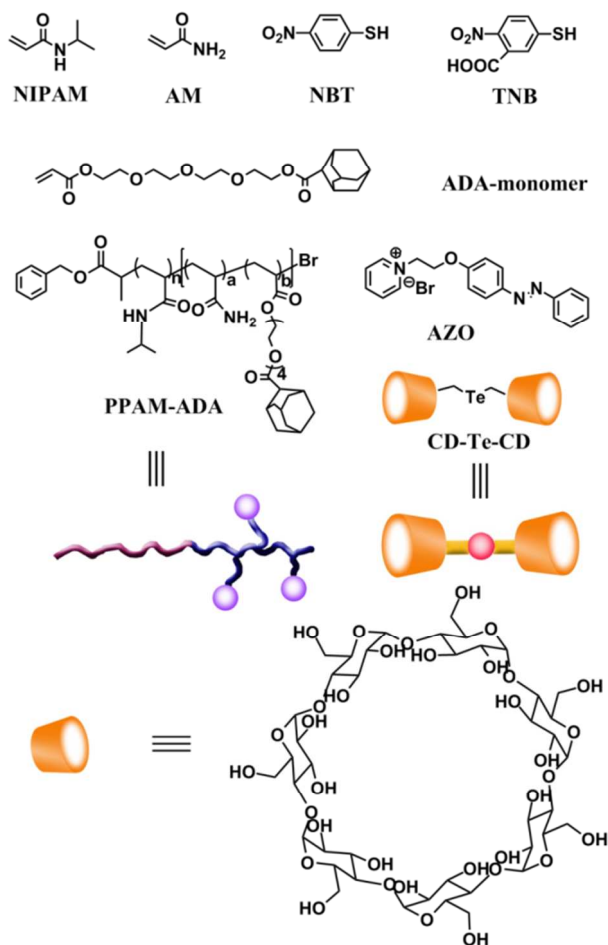

Fig. 2 The structures of NIPAM, AM, **ADA-comonomer**, adamantane-containing guest block copolymer (**PPAM-ADA**), **CD-Te-CD** and substrates (NBT, TNB).

As a thermally sensitive polymer, PNIPAM undergoes a reversible volume phase transition at near-physiological temperature with the polymer subunit changing from a hydrophilic to a hydrophobic state when the temperature is above lower critical solution temperature (LCST). Therefore, the soluble block copolymer bearing PNIPAM subunit can change to amphiphilic polymer when the temperature was above LCST. As reported by our group before, the latter provide a rationale for the design of a smart artificial GPx[18,49-51]. In an effort to provide the basic information needed for the preparation of **PPAM-ADA-Te**, the temperature responsive properties of **PPAM-ADA** was investigated first. Typically, the LCST of **PPAM-ADA** was determined as 32.2°C (cf. Fig. 3 **a**). And the optical transmittance

was found to roughly 70% when the temperature was below LCST. This might be due to the hydrophobic **ADA-monomer** being anchored into the scaffold of **PPAM-ADA**. Such lower temperature dependence indicates that **PPAM-ADA** can entertain a self-assembled aggregation when the temperature is below LCST. The hydrodynamic diameters of **PPAM-ADA-Te** at 25°C confirmed this hypothesis：as shown in Fig. 4, the self-assembled aggregation behaviour with the average hydrodynamic diameters of 68 nm and 139 nm could be observed at 25°C and 35°C, respectively. Therefore, the hydrophobic microenvironment not only results from the introduction of a hydrophobic **ADA-monomer** but is also due to the hydrophobic polymer scaffold with the temperature being above LCST. Considering that a strongly hydrophobic microenvironment does not penetrate host molecule into the aggregation of **PPAM-ADA** and form the supramolecular complex, the self-assembled temperature of **PPAM-ADA-Te** was selected to be 32°C, i.e. just slightly lower than the LCST of **PPAM-ADA**. A schematic representation of this self-assembly process of **PPAM-ADA-Te** is shown in Scheme 1.
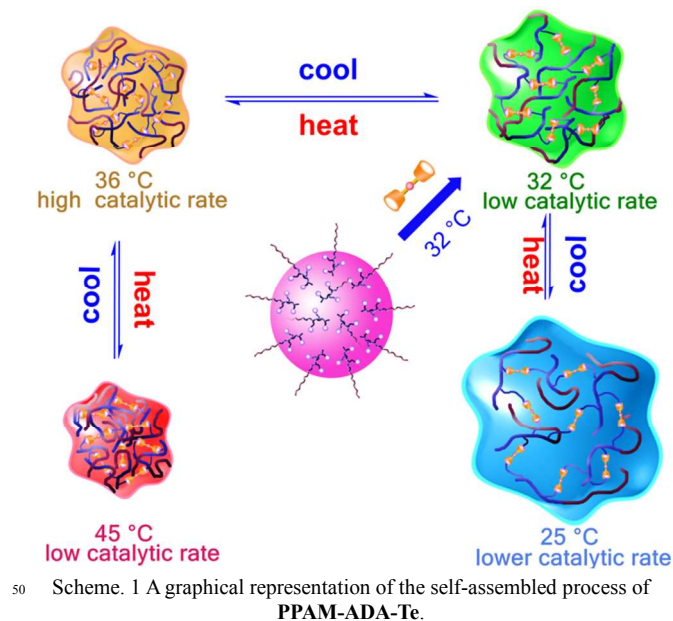
Scheme. 1 A graphical representation of the self-assembled process of **PPAM-ADA-Te**.
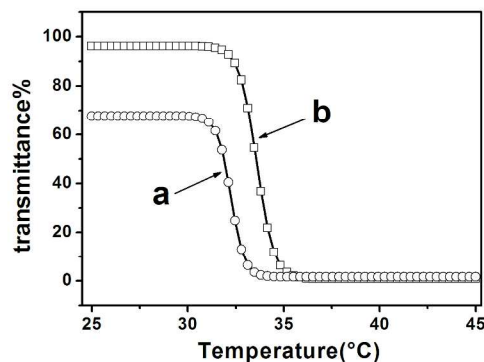

Fig. 3 Temperature dependence of optical transmittance at 600 nm obtained for pH 7.0, 50 mM PBS of (a) **PPAM-ADA**, (b) **PPAM-ADA-Te** at concentrations of 1 mg·mL^{-1}.
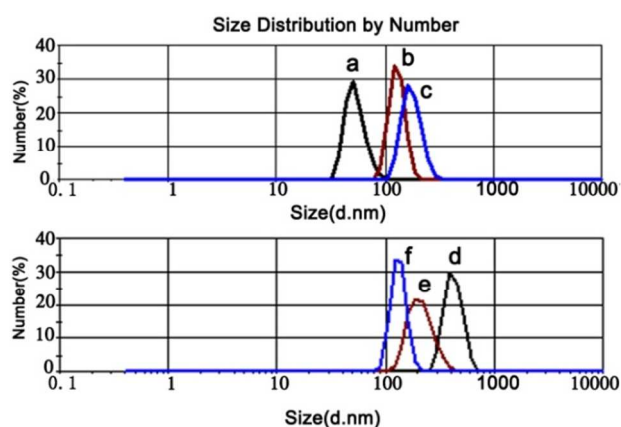
Fig. 4 Hydrodynamic diameters of **PPAM-ADA** at varying temperatures (a, 25°C; b, 35°C; c, 45°C) and hydrodynamic diameters of **PPAM-ADA-Te** at varying temperatures (d, 25°C; e, 35°C; f, 45°C) determined using a Malvern ZETAS12-ERNANOSERIES instrument.

Characterization of PPAM-ADA-Te

The formation of host-guest supramolecular complex in the network of **PPAM-ADA-Te** has been confirmed by optical transmittance, DLS, NMR, SEM, and TEM. The data shown in Fig. 3 suggests that the temperature dependence of optical transmittance of **PPAM-ADA-Te** (curve **b**) is different than that of **PPAM-ADA** (curve **a**). The LCST of **PPAM-ADA-Te** was found to be 33.6°C, which proved to be higher than that of **PPAM-ADA** (32.2°C). The optical transmittance of **PPAM-ADA-Te** was found to be higher than that of **PPAM-ADA** when the temperature was below the LCST of **PPAM-ADA**. Interestingly, **PPAM-ADA** proves to be a more hydrophobic polymer since the hydrophobic **ADA-monomer** is present in the scaffold. Compared with the hydrophobic **PPAM-ADA**, **PPAM-ADA-Te** proved to be more hydrophilic as the hydrophobic **ADA-monomer** was included in the cavity of **CD-Te-CD** during the formation process of this supramolecular complex. Therefore, the formation of the supramolecular complex in the microgel network plays an important role in enhancing of optical transmittance and increasing LCST of **PPAM-ADA-Te**. In other words, the difference of optical transmittance and LCSTs between **PPAM-ADA-Te** and **PPAM-ADA** could provide evidence for the formation of a self-assembled structure of **PPAM-ADA-Te**.
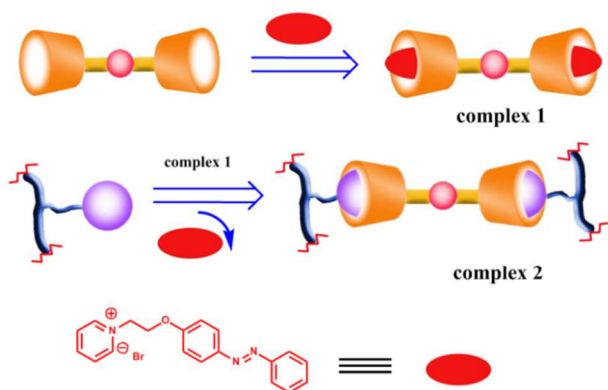
Scheme. 2 A graphical representation of the competitive complex mechanism using **AZO** as an indicator.

To further prove the successful formation of the host-guest complex in **PPAM-ADA-Te**, NMR assay was carried out using **AZO** as a competitive guest. Compared with the host-guest interaction between **AZO** and cyclodextrin, the host-guest interaction between adamantane (in **PPAM-ADA**) and cyclodextrin (in **CD-Te-CD**) was much stronger. And the host-guest complex between **PPAM-ADA** and **CD-Te-CD** was more stable. Therefore, it is believed that adamantane in **PPAM-ADA** could supplant **AZO** from the cave of cyclodextrin of **CD-Te-CD** even if the complex between **AZO** and cyclodextrin forms preferentially. **AZO** can therefore act as the indicator to confirm the host-guest complex between **PPAM-ADA** and **CD-Te-CD**. A schematic representation for this competitive complex mechanism using **AZO** as an indicator is shown in Scheme 2. Three individual sets of ^{1}H NMR spectra are shown in Fig 5.
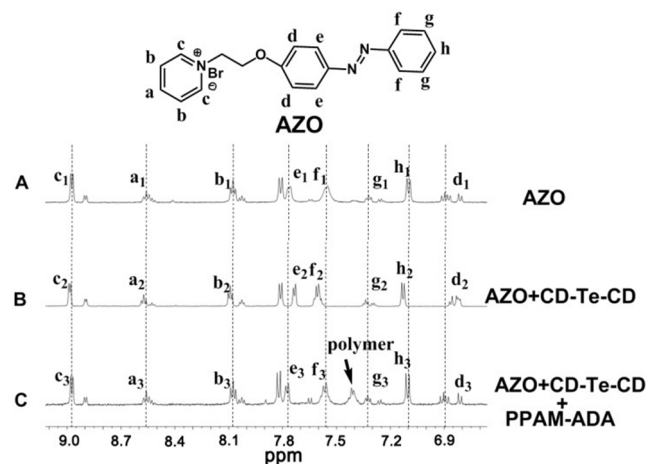
Fig. 5 ^{1}H NMR spectra of A) proton signals of aromatic ring in pure **AZO**, B) proton signals of aromatic ring in the binary system of **AZO/CD-Te-CD**, C) aromatic ring in the ternary system of **AZO/CD-Te-CD/PPAM-ADA** in D_2O

The three ^{1}H NMR spectra are shown in Fig 5 **A**, Fig 5 **B** and Fig 5 **C**. The proton shifts of aromatic ring in pure **AZO**, binary system of **AZO/CD-Te-CD** and ternary system of **AZO/CD-Te-CD/PPAM-ADA** in D_2O are respectively illustrated. By comparison of the spectrum in Fig 5 **B** with the spectrum in Fig 5 **A**, it was found that proton signals of c_2, a_2, b_2, f_2, g_2, h_2 shifted to low field, suggesting that these protons in binary system were exposed to water moderately and were not included by cyclodextrin. It was also found that proton signals of d_2 and e_2 shifted to high field, suggesting that these protons were included in the hydrophobic cavity of cyclodextrin and the proton signals were shielded. These results provide evidence for **AZO** being included in the cavity of **CD-Te-CD**, and the successful formation of a complex consisting of **AZO** and **CD-Te-CD**. the latter finding is also on par with a previously published report that investigated the formation mechanism of a host-guest complex between **AZO** and another cyclodextrin species[64]. Subsequently, a ternary system of **AZO/CD-Te-CD/PPAM-ADA** was obtained by adding **PPAM-ADA** to the binary system of **AZO/CD-Te-CD** (seen in Fig. 5 **C**). It was found that the protons in the aromatic ring of this ternary system exhibited the same chemical shifts as those in neat AZO, suggesting that **AZO** was not included in the cavity of **CD-Te-CD** and the complex of

AZO and **CD-Te-CD** does indeed not form under these conditions. In other words, this observation confirmed the hypothesis that **PPAM-ADA** could supplant **AZO** from the cave of **CD-Te-CD**. Furthermore, a complex of **PPAM-ADA** with
5 **CD-Te-CD** also indeed formed.

Analyses including DLS, SEM and TEM have been performed in order to provided detailed information on the aggregation morphology, which is essential for the investigation of catalytic mechanism involving artificial GPx. DLS was used in
10 an effort to determine the temperature dependence of hydrodynamic diameters of **PPAM-ADA** and **PPAM-ADA-Te**. As displayed in Fig. 4, the hydrodynamic diameters of **PPAM-ADA** at 25°C (curve **a**), 35°C (curve **b**) and 45°C (curve **c**) were found to be 68 nm, 139 nm and 197 nm, respectively. However,
15 the hydrodynamic diameters of **PPAM-ADA-Te** at 25°C (curve **d**), 35°C (curve **e**) and 45°C (curve **f**) were found to be 441 nm, 244 nm and 141 nm, respectively. Truly remarkable is the fact that the hydrodynamic diameter of **PPAM-ADA-Te** at 25°C (curve **d**) proves to be significantly different from that of **PPAM-**
20 **ADA** at 25°C (curve **a**). Considering that **PPAM-ADA** is a block copolymer including a hydrophobic **ADA-monomer** and **PPAM-ADA-Te** proves to be a crosslinked polymer network, the different hydrodynamic diameters of **PPAM-ADA-Te** compared to **PPAM-ADA** can be explained by their different polymer
25 structures. Similarly, this observation provides further evidence for the successful formation of a crosslinked supramolecular microgel with larger hydrodynamic diameter. Additionally, the hydrodynamic diameter of **PPAM-ADA-Te** decreases upon a temperature increases from 35°C to 45°C, which might be caused
30 by temperature responsive property of PNIPAM block in **PPAM-ADA-Te**. For naturally occurring enzymes, it was found that minor changes in the structure of the enzyme resulted in a dramatic change in catalytic activity. Therefore, the temperature responsive change of aggregation morphology of **PPAM-ADA-**
35 **Te** might provide important insight into the regulation mechanism of the catalytic activity.

The actual morphology of **PPAM-ADA-Te** has been observed by SEM (cf. Fig. 6). Here, evidence for the presence of spherical nanoparticles, about 180 nm in average diameter, has
40 been provided. The dimensions of these spherical nanoparticles observed from SEM were found to be smaller than that observed by DLS. This finding might be due to the fact that the Zetasizer Nano instrument reports the average hydrophobic diameter with the contribution of swollen corona of nanoparticles. Additionally,
45 TEM assay was further used to reveal the detailed morphologies of the spherical nanoparticles (see in Fig. 7). Here, the diameters of spherical nanoparticles were found to be in good agreement with the ones obtained by SEM assay. Particularly, one characteristic property of microgel structures, i.e. the presence of
50 a series of minuscule cavities, has been observed by TEM. The similar structure have been reported in our previous report[17]. Such unique structural characteristics of **PPAM-ADA-Te** provide further evidence for the formation of a supramolecular microgel based on the host-guest self-assembly of **PPAM-ADA** with **CD-**
55 **Te-CD**.

Further studies comparing the detailed microgel structure of **PPAM-ADA-Te** with that of **Microgel GPx**[49] and **SM-Te**[17] revealed that very similar structural aggregates for all three

analogues can be found on a nano-scaled. A slight structural
60 change indeed results in a dramatic change in catalytic activity of the artificial enzyme system. The similar structural aggregates potentially represent three microgel-scaffold artificial GPxs offering two distinct properties:(1) the structural aggregates might exhibit a similar temperature responsive catalytic
65 behaviour and (2) the structural aggregates could provide a rationaleforthe influence of the crosslinker on the catalytic mechanism.
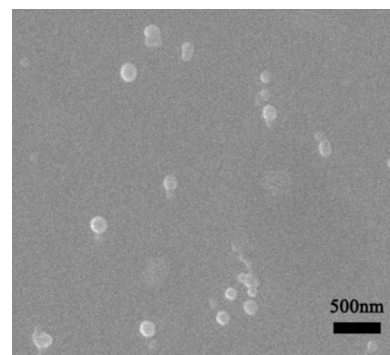

Fig.6 SEM image for **PPAM-ADA-Te** at 36°C
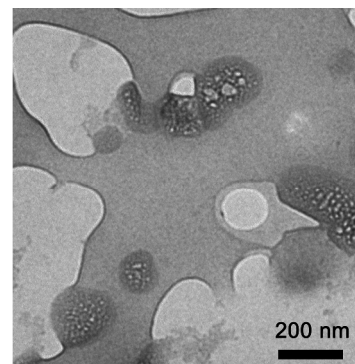

70

Fig.7 TEM image for **PPAM-ADA-Te** at 36°C

Catalytic behaviour of PPAM-ADA-Te

In order to evaluate the catalytic behaviour of **PPAM-ADA-Te**, the catalytic activity in the reduction of cumene hydorperoxide
75 (CUOOH) by 3-carboxyl-4-nitrobenzenethiol (TNB) has been determined. The experiment has been carried out according to a modified protocol reported by Hilvert *et al* using TNB as a GSH alternative (cf. Fig. 8)[6]. The relative activity was obtained under the assumption that only one catalytic center (i.e. Te-monomer)
80 in the **PPAM-ADA-Te** serves as one active site of enzyme. The catalytic reaction was initiated by the addition of hydroperoxide and the corresponding catalytic rates were summarized in Table 1. Herein, the catalytic activities of various tellurium-containing GPx mimics based on CUOOH and TNB as substrates were also
85 illustrated, which were uniformly employed to evaluate the catalytic ability of various GPx mimics. As displayed in Table 1, a slight enhancement in the catalytic rate was observed (v_0=0.010 μM·min^{-1}) when a traditional small molecule artificial GPx (i.e.PhSeSePh) was used under the identical conditions.
90 Noticeably, **PPAM-ADA-Te** exhibited a significantly enhanced catalytic rate (v_0=18.06 μM·min^{-1}). The maximum catalytic rate of **PPAM-ADA-Te** was determined to be similar to other GPx mimics (e.g. **CD-Te-CD**, **Telluro-micelle catalyst** and **SGPx).**

The maximum catalytic rate of **PPAM-ADA-Te** was found to be slightly lower than the catalytic rate of polystyrene nanoparticle GPx mimic (i.e. **PN1**). However, **SGPx** and **PN1** have been modified to contain three catalytic elements (catalytic center, binding site and hydrophobic environment), whereas **PPAM-ADA-Te** has been modified to contain merely two catalytic elements (catalytic center and hydrophobic environment). In light of this finding, **PPAM-ADA-Te** has been determined to be an excellent GPx mimic with reasonably high catalytic activity. Furthermore, the maximum catalytic rate of **PPAM-ADA-Te** was found to be higher than that of other tellurium-containing supramolecular GPx mimic (e.g. **Copolymer Vesicles GPx mimic** and **Bifunctional enzyme model**). Among the temperature responsive GPxs (**Microgel_max**, **SM-Te_max**, **Star-shaped pseudo-block copolymer catalyst**, **PNIPAM-CD-g-Te**,

and **PPAM-ADA-Te** in this work), **PPAM-ADA-Te** features the highest catalytic activity. In particular, compared with two microgel GPxs , i.e. **SM-Te** and **Microgel GPx**, the catalytic activity of **PPAM-ADA-Te** was found to be significatnly increased by 222.5% and 123.2%, respectively. This finding reflects the fact that **PPAM-ADA-Te** displays temperature responsive properties with similar catalytic activity than other non-responsive GPx mimics. Furthermore, **PPAM-ADA-Te** features the most advantageous catalytic activity among all temperature responsive GPx mimics. The high catalytic activity of **PPAM-ADA-Te** was found to be due to the reasonable design of the microgel scaffold. Further information for the latter hypothesis can be found in the subsection entitled *Catalytic mechanism of **PPAM-ADA-Te***.
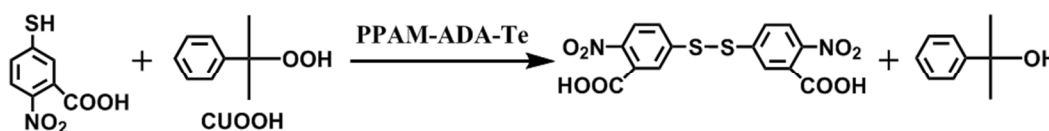

Fig. 8 Determination of GPx catalytic rate for the reduction of CUOOH using 3-carboxyl-4-nitrobenzenethiol (TNB) as substrate.

Table 1 The initial rates (v_0) for the reduction of ROOHs by ArSH in the presence of **PPAM-ADA-Te** and other tellurium-containing catalysts.

Catalyst	Temperature (°C)	ArSH	ROOH	v_0 (mM·min^{-1}) [a]
PPAM-ADA-Te	30	TNB	CUOOH	2.92
PPAM-ADA-Te	32	TNB	CUOOH	3.91
PPAM-ADA-Te	33	TNB	CUOOH	4.76
PPAM-ADA-Te	34	TNB	CUOOH	7.24
PPAM-ADA-Te	35	TNB	CUOOH	11.14
PPAM-ADA-Te	36	TNB	CUOOH	18.06
PPAM-ADA-Te	38	TNB	CUOOH	17.13
PPAM-ADA-Te	40	TNB	CUOOH	15.51
PPAM-ADA-Te	43	TNB	CUOOH	13.61
PPAM-ADA-Te	30	NBT	CUOOH	2.86
PPAM-ADA-Te	32	NBT	CUOOH	3.74
PPAM-ADA-Te	33	NBT	CUOOH	4.85
PPAM-ADA-Te	34	NBT	CUOOH	8.37
PPAM-ADA-Te	35	NBT	CUOOH	17.95
PPAM-ADA-Te	36	NBT	CUOOH	29.51
PPAM-ADA-Te	38	NBT	CUOOH	31.13
PPAM-ADA-Te	40	NBT	CUOOH	28.96
PPAM-ADA-Te	43	NBT	CUOOH	26.83
PPAM-ADA-Te	45	NBT	CUOOH	23.15
Microgel_max [b]	32	TNB	CUOOH	8.09
SM-Te_max [c]	38	TNB	CUOOH	5.60
PhSeSePh	36	TNB	CUOOH	0.010
CD-Te-CD	36	TNB	CUOOH	16.54
Telluro-micelle catalyst [d]	37	TNB	CUOOH	15.11
PN1 [e]	37	TNB	CUOOH	24.1
Copolymer Vesicles GPx mimic [f]	25	TNB	CUOOH	9.04
Bifunctional enzyme model [g]	25	TNB	CUOOH	9.60
Star-shaped pseudo-block copolymer catalyst [h]	37	TNB	CUOOH	8.11
SGPx [i]	36	TNB	CUOOH	18.75
PNIPAM-CD-g-Te [j]	35	TNB	CUOOH	6.23
PPAM-ADA	36	TNB	CUOOH	ND
Corsslinker 1 [k]	36	TNB	CUOOH	1.80
Corsslinker 2	36	TNB	CUOOH	1.89
Corsslinker 3	36	TNB	CUOOH	1.93

[a] The initial rates (v_0) for the reduction of ROOHs (250μM) by ArSH (150μM) were determined at pH 7.0 (50 mM PBS). the initial rate of reaction was corrected for the spontaneous oxidation.
[b] the microgel artificial GPx (**Microgel**) constructed in our previous report[49].
[c] the supramolecualr microgel artificial GPx (**SM-Te**) constructed in our previous report[17].
[d] the GPx mimic based on tellurium-based polymeric micelle[46].
[e] the GPx mimic based on polystyrene nanoparticle via microemulsion polymerization[48].
[f] the GPx mimic based on polymer-based vesicles of polystyrene-block-poly[tri(ethylene glycol) methyl ether acrylate]s[47].
[g] the bifunctional supramolecular artificial enzyme with both SOD and GPx onstructed by the self-assembly of the Mn(III)meso-tetra[1-(1-adamantyl methyl ketone)-4-pyridyl] porphyrin (MnTPyP-M-Ad) and cyclodextrin-based telluronic acid[34].
[h] the modulatory bifunctional artificial enzyme with both SOD and GPx activities based on smart star-shaped pseudo-block copolymer[38].
[i] the smart supramolecular artificial GPx with temperature responsive catalytic activity based on host–guest interaction and a blending process[18].
[j] the supramolecular GPx mimic based on asupramolecular graft copolymer[40].
[k] the solution of assay system of catalytic rate consisted of DMF and PBS(v:v=1:9).
ND : no detectable GPx activity.

In order to reveal the temperature responsive properties of **PPAM-ADA-Te**, the catalytic rates have been determined in

TNB and NBT assay systems using CUOOH as substrate at various temperatures (cf. Table 1). In general, according to Arrhenius equation, the reaction rates for the majority of temperature-activated reactions are enhanced as temperature increases. However, the catalytic activity trend of **PPAM-ADA-Te** seems to somewhat contradict this general trend. To outline the temperature responsive behaviour of **PPAM-ADA-Te**, a thermally responsive catalytic activity curve was obtained by plotting the catalytic reaction rates versus the temperatures (cf. Fig. 9). It was found that the catalytic activity slowly increased as the temperature rises (below 32°C). However, the catalytic activity increases significantly as the temperature increases from 32°C to 36°C. The maximum catalytic rate in the TNB assay system, i.e. 18.06 μM·min^{-1}, was obtained at 36°C. Furthermore, it was found that a sharp decrease in catalytic activity was observed as the temperature increased further. Elucidation on the temperature responsive catalytic mechanism is presented in the subsection entitled *Catalytic mechanism of PPAM-ADA-Te*. As shown in Fig. 10, the saturation kinetics of **PPAM-ADA-Te** for the peroxidase reaction were studied at the individual concentrations of CUOOH, indicating that **PPAM-ADA-Te** exhibited a typical saturation kinetics behaviour and serves as a catalyst for the peroxidase reaction. In the TNB assay system, the kinetic parameters were determined as follows: V_{max}=67.57 μM·min^{-1}, k_{cat}^{app} =67.57 min^{-1}, $K_{m\ CUOOH}$ =736.5 μM, $k_{cat}^{app}/K_{m\ CUOOH}$ =9.17×10^4 M^{-1}·min^{-1}, and the turnover number per catalytic center tellurium was calculated to be 67 min^{-1}.
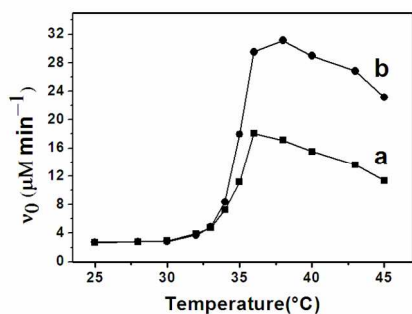

Fig. 9 Plots of the catalytic rates of **PPAM-ADA-Te** versus temperatures during the catalytic reduction of CUOOH (0.25 mM) by TNB (0.15 mM, curve **a**) and NBT (0.15 mM, curve **b**).
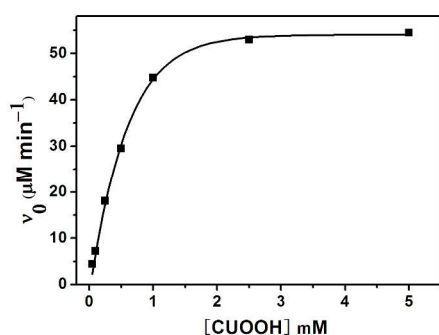

Fig. 10 Plots of initial rates at different concentrations of CUOOH in the presence of **PPAM-ADA-Te**. The initial concentration of TNB was fixed to 0.15 mM, The concentrations of CUOOH were 0.05, 0.10, 0.25, 0.5, 1, 2.5 and 5 mM, respectively.

As the scaffold of **PPAM-ADA-Te** represents a dynamic self-assembled structure, the stability of this system has been evaluated. Considering that slight structural alterations could result in a dramatic change in catalytic activity, the catalytic activity of **PPAM-ADA-Te** was used as a measure to evaluate the structural stability. Here, the changes of catalytic activity (curve **a**) and hydrodynamic diameters (curve **b**) of **PPAM-ADA-Te** were investigated upon addition of an adamantane scaffold (i.e. amantadine hydrochloride), serving as a guest molecule (cf. Figure11). The catalytic activity was slightly changed when the molar ratio of amantadine hydrochloride to **CD-Te-CD** was below 0.1. And the hydrodynamic diameters of of **PPAM-ADA-Te** was also slightly changed under this condition. The observation indicates that the formation of a complex of adamantane in **PPAM-ADA** and cyclodextrin in **CD-Te-CD** is slightly influenced by excess amantadine hydrochloride (0.1 times). Likewise, this finding provides further evidence for the efficient formation of a stable self-assembled structure of **PPAM-ADA-Te**. As the concentration of excess amantadine hydrochloride increases, the catalytic activity gradually decreases and the hydrodynamic diameters gradually increase. It suggested the stable self-assembled structure was destroyed to some extent by excess amantadine hydrochloride. Herein, excess amantadine hydrochloride might supplant adamantane in **PPAM-ADA** from the cave of **CD-Te-CD** through competitive host-guest interaction to a certain degree. This observation reflected the dynamic self-assembled property of **PPAM-ADA-Te**. It was concluded that the self-assemble structure of **PPAM-ADA-Te** was stable as the scaffold for artificial GPx. This remarkable stability provides a further incentive to investigate the catalytic mechanism involving **PPAM-ADA-Te** as described below.
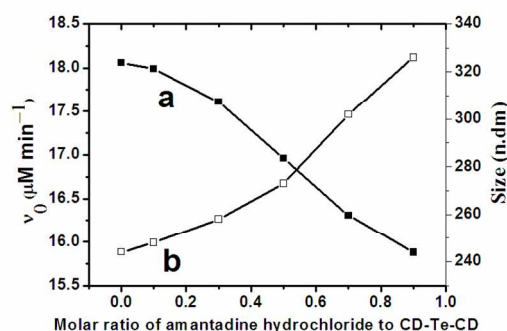

Fig.11 The changes of catalytic activity (curve **a**) and hydrodynamic diameters (curve **b**) of **PPAM-ADA-Te** under the presence of excess amantadine hydrochloride.

Catalytic mechanism of PPAM-ADA-Te

We suggested that both hydrophobic microenvironment and the crosslinker in a supramolecular microgel network played important roles in enhancing and altering the temperature responsive catalytic behaviour. Previously, we showed that modifications in the hydrophobic microenvironment are important for the temperature responsive catalytic behaviours of **Microgel GPx**[49] and **SM-Te**[17]. The temperature responsive catalytic behaviour is illustrated in Fig.9. The temperature responsive mechanism can be investigated using a TNB assay

system (cf. Fig. 9 **a**). Through combination of the changes in optical transmittances (cf. Fig. 3 **b**), the changes in hydrodynamic diameters in (cf. Fig. 4, curve **d**, **e** and **f**) as well as the changes in catalytic rates (cf. Fig. 9 **a**), it was found that the change trend for the catalytic rate was in good agreement with the change trends for the optical transmittance and hydrodynamic diameters. Particularly, the pivotal catalytic factor, hydrophobic microenvironment is irrelevant at a temperature below 32°C, **PPAM-ADA-Te** exhibits a weak substrate binding ability and a low catalytic rate. Presumable, the microgel scaffold of **PPAM-ADA-Te** gradually de-swells when the temperature rises above 32°C. The optical transmittance decreases and the average hydrodynamic diameter is found to be 244 nm at 35°C. Likely, a hydrophobic microenvironment was preliminarily formed in the deswelled microgel scaffold. The substrate binding ability and catalytic rate were remarkably enhanced under these conditions. However, a sharp decrease in catalytic activity has been observed as the temperature was continuously increased above 36°C. The hydrophobicity of PNIPAM in **PPAM-ADA-Te** further increases under these conditions, inhibiting the mobility of the substrates to permeate into the active site of **PPAM-ADA-Te** in order to complete the GPx catalytic reactions. Therefore, the catalytic rates decrease significantly as the efficient binding ability for the substrates becomes too low.

The catalytic rates have been measured in different assay systems using a variety of substrates(cf. Fig. 12). Furthermore, the systems have been used to investigate the influence of hydrophobic microenvironment. In general, the rate constants of the spontaneous reaction between a hydroperoxide and thiol vary in magnitude with $k(H_2O_2) > k(CUOOH)$[12]. However, it was found that a higher catalytic rate was achieved when CUOOH was used as the corresponding substrate (cf. Fig. 12, A>C, or B>D). This significant difference is also reflected in the fact that the hydrophobic microenvironment allows the hydrophobic substrate CUOOH to approach the active site in **PPAM-ADA-Te** in order to complete this enzymatic reaction. This finding also suggests that the influence of the hydrophobic microenvironment plays an important role in the determination of the catalytic rates.

To further study the influence of the relative pore size during the change process of the hydrophobic microenvironment, the temperature responsive behaviour was determined in a NBT assay system (cf. Fig. 9 **b**). by comparison of the temperature responsive behaviour of **PPAM-ADA-Te** (cf. Fig. 9) with the previous reported temperature responsive GPx mimics[17, 18, 38, 40, 49], it was found that **PPAM-ADA-Te** features a similar temperature responsive mechanism. However, in comparison to the TNB assay system (cf. Fig. 9 **a**), a higher catalytic activity has been observed upon using the NBT assay system (cf. Fig. 9 **b**). Particularly, **PPAM-ADA-Te** still exhibits a high catalytic activity in the NBT assay system even through the temperature increases above 38°C. However, a significantly decreased catalytic activity has been observed in the TNB assay system under the same condition. This conflicting finding is most likely due to molecular size difference between TNB and NBT. The latter proves to be smaller than TNB owing to the lack of a carboxyl function group. This in turn means that NBT can access the active sit in the cores of **PPAM-ADA-Te** more easily and the GPx catalytic reaction can therefore proceed with higher catalytic

activity. This observed phenomenon is also in good agreement with the finding outlined in Fig. 12. A higher catalytic rate can be observed at 36°C when NBT is being used as the substrate (cf. Fig. 12, A<B, or C<D). This influence of the different pore size on the catalytic activity goes hand in hand with the change of the hydrophobic microenvironment. Therefore, the observations outlined above provide evidence that changing the hydrophobic microenvironment is important for regulating the GPx catalytic rate.
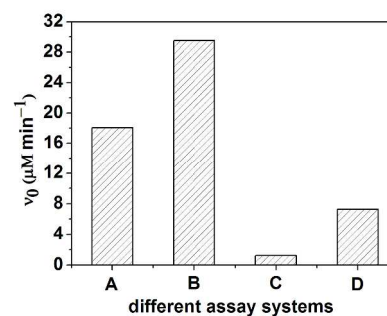
Fig. 12 The initial rates (v_0) for the reduction of hydroperoxides (250 μM) by thiol TNB and NBT (150 μM) in the presence of **PPAM-ADA-Te** at pH 7.0 (50 mM PBS) and 36°C. (A) CUOOH, TNB; (B) CUOOH, NBT; (C) H_2O_2, TNB; (D) H_2O_2, NBT.

The influence of the crosslinker in a supramolecular microgel network on altering the temperature responsive catalytic behaviour has also been studied. In previously published reports[8-12, 18, 38, 40, 49], it was found that the compounds containg a binding site or hydrophobic environment (e.g. quaternary ammonium salt, molecules with a hydrophobic cavity, arginine, etc.) could improve the catalytic ability of GPx mimics. The three crosslinkers units used are illustrated in Fig.1 and have not been modified with a binding site or hydrophobic environment. Therefore, merely a slight influence of the different functional groups has been observed, which has also been confirmed through the determination of the catalytic activities of the three crosslinkers (cf. Table 1). The catalytic activities of **Corsslinker 1**, **Corsslinker 2** and **Corsslinker 3** were found to be 1.80 μM·min^{−1}, 1.89 μM·min^{−1}and 1.93 μM·min^{−1}, respectively. Additionally, no catalytic activity of the guest polymer scaffold (i.e. **PPAM-ADA**) could be detected. These controlled experiments provide the foundation for the investigating the crosslinker influence on altering of the temperature responsive catalytic behaviour.

Three characteristic temperature responsive behaviours have been found in **Microgel GPx**, **SM-Te** and **PPAM-ADA-Te** (cf. Fig. 13). The maximum catalytic rate of **PPAM-ADA-Te** was found to be higher than that of **Microgel GPx** and **SM-Te**. As illustrated in Fig. 1, the length of **Corsslinker 3** in **PPAM-ADA-Te** consisting of **CD-Te-CD** and **ADA-monomer**, proves to be in between the corresponding lengths of **Corsslinker 1** and **Corsslinker 2**. And the maximum catalytic rate of **PPAM-ADA-Te** shows that the length of **Crosslinker 3** is indeed appropriate, enabling the substrates to approach the active sites in **PPAM-ADA-Te** in a more efficient fashion..

Furthermore, the temperatures corresponding to the individual maximum catalytic rate of **Microgel GPx**, **SM-Te** and **PPAM-**

ADA-Te were found to be different. The maximum catalytic rates of **Microgel GPx**, **PPAM-ADA-Te** and **SM-Te** were obtained at 32°C, 36°C and 38°C, respectively. The increasing trend of the crosslinker length was in agreement with the increasing trend of temperature corresponding to the maximum catalytic rate. The length of the crosslinker in a supramolecular microgel network therefore plays an improtant role in altering the temperature responsive catalytic behaviour.

The catalytic activity change trends were also found to be different. The catalytic rate of **Microgel GPx** decreases as the temperature increases above 32°C. However, for **SM-Te** and **PPAM-ADA-Te**, the bell-shaped catalytic activity change curves have been observed. The distinct differences between **Microgel GPx** and **PPAM-ADA-Te** or **SM-Te** are most likely due to the different positions of the crosslinker. For **Microgel GPx**, the crosslinker and catalytic center were anchored to the PNIPAM scaffold. For **PPAM-ADA-Te** or **SM-Te**, the crosslinker and catalytic center can be found at the hydrophilic PAM block. Therefore, the hydrophobic microenvironment in **Microgel GPx** was more prominently enhanced and the pores were found to be contracted tightly as the temperature rises above 32°C. As the temperature increases above the corresponding LCST, the access of the substrates to the active sites is being impeded and the catalytic rate of **MicrogelGPx** decreases accordingly. Therefore, the position of crosslinker in a supramolecular microgel network is found to be a crucial factor when altering the temperature responsive catalytic behaviour. Moreover, although the change trend of **SM-Te** and **PPAM-ADA-Te** was found to be similar, the maximum catalytic rate of **PPAM-ADA-Te** has been shown to be far higher than that of **SM-Te**. Therefore, it can be concluded that that **Crosslinker 3** is a more suitable crosslinker unit for enhancing the catalytic rate compared to, e.g. **Crosslinker 2**.

In summary, both the hydrophobic microenvironment and the crosslinker in a supramolecular microgel network play critical roles in enhancing and altering the temperature responsive catalytic behaviour.
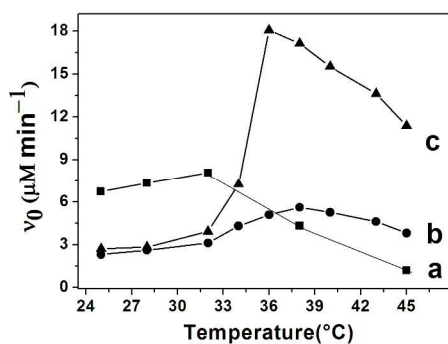

Fig. 13 Plots of the catalytic rates of **Microgel GPx**[49] (curve **a**), **SM-Te**[17] (curve **b**), and **PPAM-ADA-Te** (curve **c**) versus temperatures during the catalytic reduction of CUOOH.

Conclusions

The design and efficient synthesis of a smart artificial GPx (i.e. **PPAM-ADA-Te**) with high catalytic activity based on a supramolecular microgel has been carried out. **PPAM-ADA-Te** was prepared based on a supramolecular host-guest self-assembly process involving **CD-Te-CD** and **PPAM-ADA**. Noteworthy, **PPAM-ADA-Te** not only exhibits a significant temperature responsive catalytic activity but also features a typical saturation kinetics behaviour, similar to that of a natural enzyme catalyst. Compared with previously reported **SM-Te** and **Microgel GPx**, the catalytic activity of **PPAM-ADA-Te** was significantly increased by 222.5% and 123.2%, respectively. It was found that both the hydrophobic microenvironment and the crosslinker in a supramolecular microgel network played critical roles in enhancing and altering the temperature responsive catalytic behaviour. The successful preparation of **PPAM-ADA-Te** not only provides a novel method for the synthesis of microgel artificial GPx with high catalytic activity but also provides invaluable information for the development of intelligent antioxidant drugs.

Acknowledgments

Notes and references

a *School of Chemistry and Chemical Engineering, Guangxi University, Na nning 530004, China; Tel: +86–18290193615; E-mail: yinyanzhen2014 @163.com; Tel: +86–13507711971; E-mail: huangzq@gxu.edu.cn;*
b *Guangxi Colleges and University Key Laboratory of Beibu Gulf Oil and Natural Gas Resource Effective Utilization, College of Petroleum and Ch emical Engineering, Qinzhou University, No.89, Xihuan Nanlu, Qinzhou 535000, People's Republic of China. Tel: +86–0777–2807226; E-mail: ji aoshufei2013@163.com*

1   H. Sies, ''Oxidative Stress: Introductory Remarks'', in *Oxidative Stress*; Sies, H., Ed.; Academic Press:London ,1985, p. 1.
2.   H. Sies, *Angew. Chem., Int. Ed. Engl.,* 1986, **25**, 1058-1071.
3.   H. Sies, *Experimental physiology*, 1997, **82**, 291-295.
4.   L. Flohé, G. Loschen, W. A. Günzler and E. Eichele, *Hoppe-Seyler's Z Physiol. Chem.*, 1972, **353**, 987-999.
5.   O. EPP, R. LADENSTEIN and A. WENDEL, *Eur. J. Biochem. ,* 1983, **133**, 51-69.
6.   Z. P. Wu and D. Hilvert, *J. Am. Chem. Soc. ,* 1990, **112**, 5647-5648.
7.   L. Engman, D. Stern, I. A. Cotgreave and C. M. Andersson, *J. Am. Chem. Soc. ,* 1992, **114**, 9737-9743.
8.   T. Kanda, L. Engman, I. A. Cotgreave and G. Powis, *J. Org. Chem.,* 1999, **64**, 8161-8169.
9.   J. Liu, G. Luo, S. Gao, K. Zhang, X. Chen and J. Shen, *Chem. Commun.*, 1999, **1999**, 199-200.
10.   G. Mugesh and H. B. Singh, *Chem. Soc. Rev.*, 2000, **29**, 347-357.
11.   T. G. Back and Z. Moussa, *J. Am. Chem. Soc.*, 2003, **125**, 13455-13460.
12.   Z. Dong, J. Liu, S. Mao, X. Huang, B. Yang, X. Ren, G. Luo and J. Shen, *J. Am. Chem. Soc. ,* 2004, **126**, 16395-16404.
13.   X. Huang, Y. Z. Yin, Y. Liu, X. L. Bai, Z. M. Zhang, J. Y. Xu, J. C. Shen and J. Q. Liu, *Biosens. Bioelectron.*, 2009, **25**, 657-660.
14.   X. Huang, Y. Z. Yin and J. Q. Liu, *Macromol. Biosci.*, 2010, **10**, 1385-1396.
15.   Z. Dong, Q. Luo and J. Liu, *Chem. Soc. Rev.*, 2012, **41**, 7890-7908.
16.   C. Hou, Q. Luo, J. Liu, L. Miao, C. Zhang, Y. Gao, X. Zhang, J. Xu, Z. Dong and J. Liu, *ACS Nano*, 2012, **6**, 8692-8701.
17.   Y. Z. Yin, S. F. Jiao, C. Lang and J. Q. Liu, *Soft Matter*, 2014, **10**, 3374-3385.

18. Y. Z. Yin, S. F. Jiao, C. Lang and J. Q. Liu, *RSC Adv.*, 2014, **4**, 25040–25050.
19. X. Zhang, H. Xu, Z. Dong, Y. Wang, J. Liu and J. Shen, *J. Am. Chem. Soc.*, 2004, **126**, 10556-10557
20. S. Mao, Z. Dong, J. Liu, X. Li, X. Liu, G. Luo and J. Shen, *J. Am. Chem. Soc.*, 2005, **127**, 11588-11589.
21. V. Nascimento, E. E. Alberto, D. W. Tondo, D. Dambrowski, M. R. Detty, F. Nome and A. L. Braga, *J. Am. Chem. Soc.*, 2011, **134**, 138-141.
22. Y. Fu, J. Chen, H. Xu, C. Van Oosterwijck, X. Zhang, W. Dehaen and M. Smet, *Macromol. Rapid Commun.*, 2012, **33**, 798-804.
23. Q. Luo, C. Zhang, L. Miao, D. Zhang, Y. Bai, C. Hou, J. Liu, F. Yan, Y. Mu and G. Luo, *Amino acids*, 2013, **44**, 1009-1019.
24. S. J. Balkrishna, S. Kumar, G. K. Azad, B. S. Bhakuni, P. Panini, N. Ahalawat, R. S. Tomar, M. R. Detty and S. Kumar, *Org. Biomol. Chem.*, 2014, **12**, 1215-1219.
25. Z. Huang, Q. Luo, S. Guan, J. Gao, Y. Wang, B. Zhang, L. Wang, J. Xu, Z. Dong and J. Liu, *Soft Matter*, 2014, **10**, 9695-9701
26. Z. Luo, L. Liang, J. Sheng, Y. Pang, J. Li, L. Huang and X. Li, *Bioorg. Med. Chem.*, 2014, **22**, 1355-1361.
27. P. Prabhu, B. G. Singh, M. Noguchi, P. P. Phadnis, V. K. Jain, M. Iwaoka and K. I. Priyadarsini, *Org. Biomol. Chem.*, 2014, **12**, 2404-2412.
28. T. Takei, Y. Urabe, Y. Asahina, H. Hojo, T. Nomura, K. Dedachi, K. Arai and M. Iwaoka, *J. Phys. Chem. B*, 2014, **118**, 492-500.
29. L. Wang, H. Zou, Z. Dong, L. Zhou, J. Li, Q. Luo, J. Zhu, J. Xu and J. Liu, *Langmuir*, 2014, **30**, 4013-4018.
30. R. Xiao, L. Zhou, Z. Dong, Y. Gao and J. Liu, *Chin. J. Chem.*, 2014, **32**, 37-43.
31. C. Zhang, T. Pan, C. Salesse, D. Zhang, L. Miao, L. Wang, Y. Gao, J. Xu, Z. Dong, Q. Luo and J. Liu, *Angew. Chem. Int. Ed. Engl.*, 2014, **53**, 13536-13539.
32. H. P, Xu, W. Cao and X. Zhang, *Acc. Chem. Res.,* 2013, **46**, 1647-1658.
33. X. Liu, L. A. Silks, C. Liu, M. Ollivault-Shiflett, X. Huang, J. Li, G. Luo, Y. M. Hou, J. Liu and J. Shen, *Angew. Chem. Int. Ed.*, 2009, **48**, 2020-2023.
34. S. Yu, X. Huang, L. Miao, J. Zhu, Y. Yin, Q. Luo, J. Xu, J. Shen and J. Liu, *Bioorg. Chem.*, 2010, **38**, 159-164.
35. H. Xu, J. Gao, Y. Wang, Z. Wang, M. Smet, W. Dehaen and X. Zhang, *Chem. Commun.*, 2006, 796-798.
36. H. Xu, Y. Wang, Z. Wang, J. Liu, S. Mario and D. Wim, *Chinese Sci. Bull.*, 2006, **51**, 2315-2321.
37. H. Wang, L. Wang, X. Wang, J. Xu, Q. Luo and J. Liu, *New J. Chem.*, 2011, **35**, 2632-2638.
38. L. Zhou, J. Li, Q. Luo, J. Zhu, H. Zou, Y. Gao, L. Wang, J. Xu, Z. Dong and J. Liu, *Soft Matter*, 2013, **9**. 4635-4641.
39. Y. Tang, L. Zhou, J. Li, Q. Luo, X. Huang, P. Wu, Y. Wang, J. Xu, J. Shen and J. Liu, *Angew. Chem. Int. Ed.*, 2010, **49**, 3920-3924.
40. Y. Z. Yin, S. F. Jiao, Y. Wang, R. R. Zhang, Z. F. Shi and X. X. Hu, *ChemBioChem*, 2015, **16**, 670-676.
41. Y. Wang, L. Cao, S. Guan, G. Shi, Q. Luo, L. Miao, I. Thistlethwaite, Z. Huang, J. Xu and J. Liu, *J. Mater. Chem.,* 2012, **22**, 2575-2581.
42. Z. Y. Dong, X. Huang, S. Z. Mao, K. Liang, J. Q. Liu, G. M. Luo and J. C. Shen, *Chem.-Eur. J.*, 2006, **12**, 3575-3579.
43. X. Ren, J. Liu, G. Luo, Y. Zhang, Y. Luo, G. Yan and J. Shen, *Bioconjugate Chem.*, 2000, **11**, 682-687.
44. X. Ren, Y. Xue, K. Zhang, J. Liu, G. Luo, J. Zheng, Y. Mu and J. Shen, *FEBS Lett.*, 2001, **507**, 377-380.
45. X. Huang, Z. Y. Dong, J. Q. Liu, S. Z. Mao, J. Y. Xu, G. M. Luo and J. C. Shen, *Langmuir*, 2007, **23**, 1518-1522.
46. X. Huang, Z. Y. Dong, J. Q. Liu, S. Z. Mao, G. Luo and J. C. Shen, *Macromol. Rapid Commun.*, 2006, **27**, 2101-2106.
47. Y. Z. Yin, X. Huang, C. Y. Lv, L. Wang, S. J. Yu, Q. Luo, J. Y. Xu and J. Q. Liu, *Macromol. Biosci.,* 2010, **10**, 1505-1516.
48. X. Huang, Y. Liu, K. Liang, Y. Tang and J. Liu, *Biomacromolecules*, 2008, **9**, 1467-1473.
49. X. Huang, Y. Z. Yin, Y. Tang, X. L. Bai, Z. M. Zhang, J. Y. Xu, J. Q. Liu and J. C. Shen, *Soft Matter,* 2009, **5**, 1905-1911.
50. S. J. Yu, Y. Z. Yin, J. Y. Zhu, X. Huang, Q. Luo, J. Y. Xu, J. C. Shen and J. Q. Liu, *Soft Matter*, 2010, **6**, 5342-5350.
51. Y. Z. Yin, L. Wang, H. Y. Jin, C. Y. Lv, S. J. Yu, X. Huang, Q. Luo, J. Y. Xu and J. Q. Liu, *Soft Matter* 2011, **7**, 2521-2529.
52. H. Staudinger and E. Husemann, *Berichte der deutschen chemischen Gesellschaft (A and B Series)*, 1935, **68**, 1618-1634.
53. A. Biffis, N. B. Graham, G. Siedlaczek, S. Stalberg and G. Wulff, *Macromol. Chem. Phys.*, 2001, **202**, 163-171.
54. Y. Z. Yin, Z. Y. Dong, Q. Luo and J. Q. Liu, *Prog. Polym. Sci.*, 2012, **37**, 1476-1509.
55. S. Lally, R. Liu, C. Supasuteekul, B. R. Saunders and T. Freemont, *J. Mater. Chem.,* 2011, **21**, 17719-17728.
56. R. A. Siegel, Y. Gu, M. Lei, A. Baldi, E. E. Nuxoll and B. Ziaie, *J Control Release*, 2010, **141**, 303-313.
57. J. Gu, F. Xia, Y. Wu, X. Qu, Z. Yang and L. Jiang, *J. Control. Release*, 2007, **117**, 396-402.
58. Y. Gao, C. Hou, L. Zhou, D. Zhang, C. Zhang, L. Miao, L. Wang, Z. Dong, Q. Luo and J. Liu, *Macromol. Biosci.* , 2013, **13**, 808-816.
59. S. Wiese, A. C. Spiess and W. Richtering, *Angewandte Chemie*, 2013, **125**, 604-607.
60. B. Jimenez, A. Noyola, B. Capdeville, M. Roustan and G. Faup, *Water Research*, 1988, **22**, 1253-1257.
61. L. E. Bromberg and E. S. Ron, *Adv. Drug Ddeliver. Rev*, 1998, **31**, 197-221.
62. A. Vila, A. Sánchez, K. Janes, I. Behrens, T. Kissel, J. L. V. Jato and M. a. J. Alonso, *Eur. J. Pharm. Biopharm.*, 2004, **57**, 123-131.
63. M. Ciampolini and N. Nardi, *Inorg. Chem.*, 1966, **5**, 41-44.
64. P. Wu, R. Q. Xiao, C. Q. Zhang, L. P. Zhou, Q. Luo, J. Y. Xu and J. Q. Liu, *Catal. Lett.* , 2010, **138**, 62-67.
65. Z. Y. Dong, *Investigations of substrate binding and catalytic mechanism of gluthathione peroxidase mimics*, PhD Thesis, Jilin University, 2006.
66. O. Kretschmann, C. Steffens and H. Ritter, *Angew. Chem. Int. Ed.*, 2007, **46**, 2708 –2711.
67. K. Matyjaszewski and J. Xia, *Chem. Rev.*, 2001, **101**, 2921-2990.
68. J. Wang and K. Matyjaszewski, *J. Am. Chem. Soc.*, 1995, **117**, 5614-5615.